Materials Today Energy 58 (2026) 102253

Contents lists available at ScienceDirect

Materials Today Energy

journal homepage: www.journals.elsevier.com/materials-today-energy/

Data mining the missing ordered phases of Li/Na metal oxides

Xiaozhao Liu [a], Lin Wang [a], Benjamin Cahill [a], Hui Xiong [b], Bin Ouyang [a,*], Yan Zeng [a,**]

[a] Department of Chemistry and Biochemistry, Florida State University, Tallahassee, FL, 32304, USA
[b] Micron School of Materials Science and Engineering, Boise State University, Boise, ID, 83720, USA

ARTICLE INFO

Keywords:
High-throughput screening
Density functional theory
Metal oxides
Over stoichiometric
Batteries

ABSTRACT

Data-driven discovery of Li-ion and Na-ion battery materials has been pioneered by generic materials data platforms such as the Materials Project. After decades of progress, it is timely to ask whether there remain underexplored compositional spaces. Here, we present a systematic data-mining effort to uncover missing ordered binary, ternary and quaternary Li/Na-containing metal oxides using high-throughput density functional theory (DFT). Building on 19,120 stable and metastable oxides entries from the Materials Project, we performed 13,245 additional calculations through isovalent substitutions of known ground states, experimentally reported compounds, and specific prototype structures. Our study identifies 36 new ground states within the GGA/GGA + U convex hull and 45 within the r^{2}SCAN convex hull. Additionally, we identified 840 metastable compounds from GGA/GGA + U and 979 from r^{2}SCAN that are absent in the present Materials Project databases. Moreover, we have tripled the metastable materials in compositional spaces with a molar ratio of cation/anion >1, highlighting the overlooked opportunities in this compositional space.

1. Introduction

Understanding of Li-ion and Na-ion battery materials has advanced significantly over the past decades, driven by the growing demand for an electrified society. Computational discovery of battery materials has been greatly accelerated by efforts motivated by materials genome initiative efforts [1,2], pioneered by platforms such as the Materials Project [3]. In comparison to platforms such as OQMD [4], AFlow [5], and NOMAD [6], the Materials Project provides one of the most comprehensive datasets and tools for Li-ion and Na-ion battery materials design. As a result, it has inspired numerous innovative compositional and structural discoveries [7,8] in solid state materials such as electrodes [9–13] or electrolytes [14–18]. Despite this progress, a key question remains: Are there any overlooked compositional spaces underrepresented in existing databases? These gaps not only hinder phase diagram predictions [19] but may also introduce confirmation bias in data-driven materials discovery.

In this work, we reassessed the completeness of the Materials Project's Li/Na-containing binary, ternary and quaternary oxides and employed high-throughput density functional theory (DFT) calculations to identify potential new compounds. Building on a dataset of 19,120 Li/Na-containing oxides that are stable (energy above the hull, $E_{hull} = 0$) or metastable ($E_{hull} \leq 100$ meV/atom) hosted by the Materials Project, we performed 13,245 additional DFT calculations using various strategies. While most important compositions and structures are already captured in the existing databases, our study identified 36 new ground-state compounds ($E_{hull} = 0$) using the GGA/GGA + U functional and 45 new ground-state compounds using r^{2}SCAN functional. Additionally, GGA/GGA + U-generated-phase diagrams revealed 409 ordered binary and ternary metal oxides, as well as 431 ordered quaternary metal oxides that are stable or metastable but are absent from the Materials Project (see Table S1 for the full list of 840 new metastable compounds). Using r^{2}SCAN, we observed 465 new metastable binary and ternary oxides, as well as 514 new metastable quaternary oxides (see Table S2 for the full list of 979 new metastable compounds). Notably, the compositional space with cation/anion ratios >1 remains significantly underexplored. Our data-mining efforts have effectively tripled the number of metastable materials in this region compared to the Materials Project, highlighting a promising design space for new Li-ion and Na-ion battery materials.

2. Method

The high-throughput DFT calculations were carried out using the

* Corresponding author.
** Corresponding author.
E-mail addresses: bouyang@fsu.edu (B. Ouyang), zeng@chem.fsu.edu (Y. Zeng).

https://doi.org/10.1016/j.mtener.2026.102253
Received 21 November 2025; Received in revised form 16 February 2026; Accepted 5 March 2026
Available online 6 March 2026

Vienna Ab Initio Simulation Package [20] and the projector-augmented wave (PAW) method [21,22], with spin polarization considered. A reciprocal mesh discretization of 25 $Å^{-1}$ has been used for each calculation. All calculations are initialized with ferromagnetic ordering. The convergence criteria were set as 10^{-6} eV for electronic loops and 0.02 eV $Å^{-1}$ for ionic loops. A plane wave energy cutoff of 520 eV was used for all calculations. Both GGA/GGA + U and r^{2}SCAN [23,24] calculations are performed, for GGA/GGA + U calculations, a rotationally averaged Hubbard U correction [25,26] was used to correct the self-interaction error in oxides containing Cr, Fe, Mn, Mo, and V. The U parameters were obtained from a previously reported calibration to oxide formation energies [26].

3. Results and discussion

3.1. High-throughput screening pipeline and representative structures

The high-throughput pipeline is illustrated in Fig. 1(a), comprising three pathways designed to generate potential new compounds within the targeted compositional space. The first pathway explores isovalent ion substitution on ground states in the Materials Project (MP), using both GGA/GGA + U and r^{2}SCAN-generated phase diagrams. The ground-state reference structures were selected through a systematic survey of 519 binary metal oxides in the Materials Project. These oxides span the following elements: Li, Na, K, Rb, Cs, Mg, Ca, Sr, Ba, Sc, Ti, V, Cr, Mn, Fe, Co, Ni, Cu, Zn, Y, Zr, Nb, Mo, Ru, Rh, Pd, Ag, Cd, Hf, Ta, W, Re, Os, Ir, Pt, Au, Al, Ga, In, Ge, Sn, Sb, Bi, La, Ce, Pr, Nd, Sm, Eu, Tb, Gd, Dy, Er, Ho. 32 oxides with $Fm\bar{3}m$ space group were identified, including Li_2O, Na_2O, K_2O, Rb_2O, Al_2O; MgO, CaO, SrO, BaO, ScO, TiO, CrO, NiO, CuO, ZnO, ZrO, NbO, PdO, CdO, TaO, PtO, AlO, CeO, PrO, SmO, EuO; and ZrO_2, HfO_2, BiO_2, CeO_2, PrO_2, TbO_2. Entries exhibiting unusual oxidation states (Al_2O, TaO, AlO, CeO, PrO, BiO_2, PrO_2, TbO_2) were removed. The remaining structures were retained as the ground-state references used in first pathway. The second pathway applies isovalent substitution to experimentally reported compounds in the Materials Project. In the third pathway, 44 representative prototype structures are introduced for isovalent ion substitution to address compositional regions that are not well covered by existing databases. These include 22 Li-containing prototypes listed in Table 1 and their corresponding 22 Na variants. Within the 44 prototype structures, some of them contain metals with mixed oxidation states, e.g., $LiCu_3O_3$ (Cu^+, Cu^{2+}), $Li_5Fe_4O_8$ (Fe^{2+}, Fe^{3+}), $Li_6Ni_5O_{10}$ (Ni^{2+}, Ni^{3+}). The metal species (M or M') that are investigated include M^+ (Cu^+, Ag^+), M^{2+} (Ag^{2+}, Ca^{2+}, Co^{2+}, Cu^{2+}, Fe^{2+}, Mg^{2+}, Mn^{2+}, Ni^{2+}, Pb^{2+}, V^{2+}, Zn^{2+}), M^{3+} (Al^{3+}, Bi^{3+}, Ce^{3+}, Co^{3+}, Cr^{3+}, Cu^{3+}, Fe^{3+}, Ga^{3+}, In^{3+}, Ir^{3+}, La^{3+}, Mn^{3+}, Mo^{3+}, Nb^{3+}, Ni^{3+}, Sb^{3+}, Sc^{3+}, Ti^{3+}, V^{3+}, W^{3+}, Y^{3+}), M^{4+} (Ce^{4+}, Co^{4+}, Cr^{4+}, Fe^{4+}, Ge^{4+}, Hf^{4+}, Mn^{4+}, Mo^{4+}, Ni^{4+}, Sn^{4+}, Ti^{4+}, V^{4+}, W^{4+}, Zr^{4+}), M^{5+} (Ta^{5+}, Nb^{5+}, Sb^{5+}, V^{5+}), and M^{6+} (Cr^{6+}, Mo^{6+}, W^{6+}, Te^{6+}). This selection ensures coverage of typical metal species that have been applied or have potentials in Li-ion and Na-ion battery materials. This work focusses

Table 1
22 Li-containing prototype structures with cation/anion ratio larger than one.

Prototype Structure	Materials Project ID	Prototype Structure	Materials Project ID
$LiCu_3O_3$	mp-765613	$Li_8Nb_2O_9$	mp-28030
Li_2NiO_2	mp-19308	Li_8SnO_6	mp-4527
Li_3InO_3	mp-27417	Li_8CrO_6	mp-780493
Li_3SbO_3	mp-756935	$Li_9Cr_5O_{12}$	mp-761270
Li_4GeO_4	mp-4558	$Li_{14}Mn_2O_9$	mp-770530
Li_5InO_4	mp-778877	$Li_5Fe_4O_8$	mp-754802
Li_5TaO_5	mp-755013	$Li_5V_4O_8$	mp-771611
$Li_6Hf_2O_7$	mp-770805	$Li_6Ni_5O_{10}$	mp-752908
Li_6MnO_4	mp-770533	$Li_8Ni_5O_{10}$	mp-755081
Li_6TeO_6	mp-7941	$Li_9Co_2O_8$	mp-776979
Li_7TaO_6	mp-28891	$Li_5Co_4O_8$	mp-760135

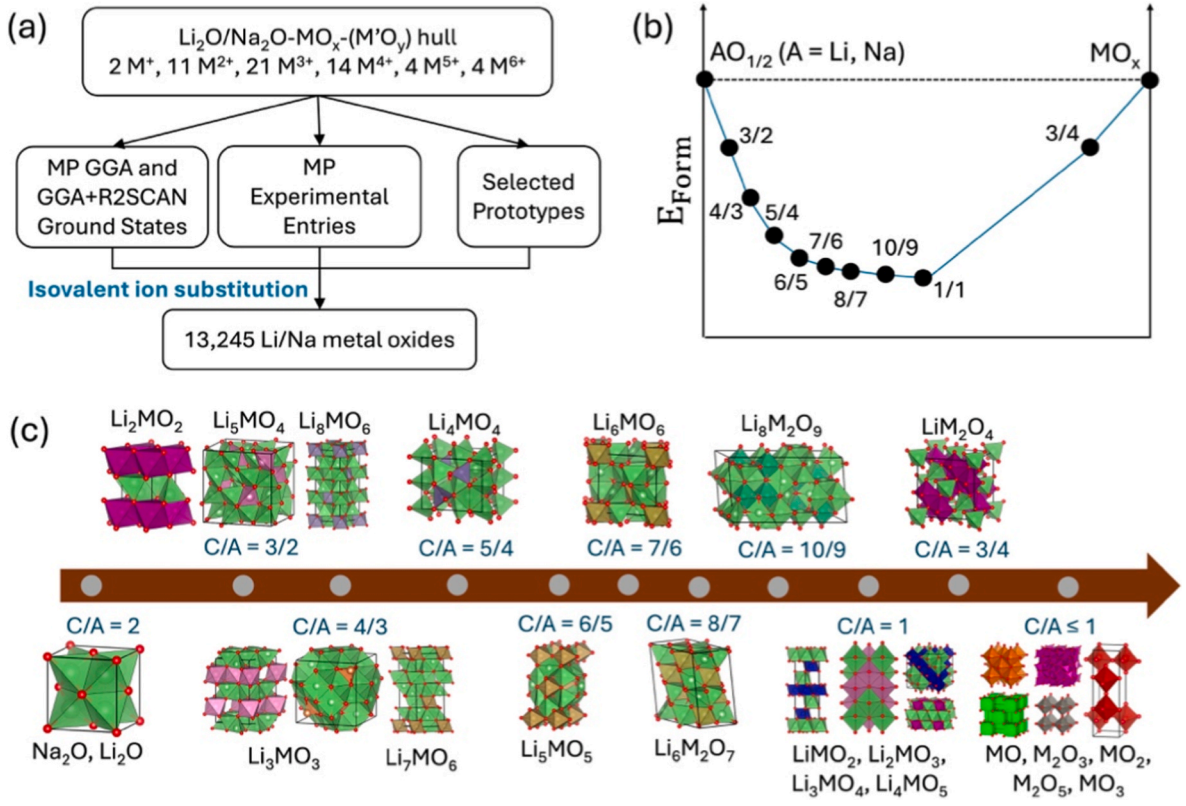

Fig. 1. (a) The pipeline of high-throughput DFT calculations for generating materials in Li_2O/Na_2O-MO_x(-M'O_y) space; (b) Illustration of the potential cation/anion ratios in the convex hull between Li_2O/Na_2O and MO_x; (c) Examples of representative structures with different cation/anion ratios.

solely on ordered forms of those materials because ordered materials are important foundation for disordered materials as they are typical low temperature competing phases of disordered materials. Meanwhile, many good battery materials are very ordered, such as $LiCoO_2$, $LiFePO_4$, $LiMn_2O_4$ etc. Overall, our workflow enhances the completeness of Li and Na oxide chemistries by systematically exploring compositional regions that are historically underrepresented in existing databases, especially those with cation to anion ratios greater than one.

As of July 2025, the Materials Project database contains relatively small numbers of compounds with cation/anion ratios greater than one. To address this gap, the selection of prototype structures in our study focuses on this compositional domain. As illustrated in Fig. 1(b) and (c), this region exhibits rich variations in potential crystal structures. Bounded by the extreme cases of antifluorite-type Li_2O and Na_2O with cation/anion ratio = 2 and the rocksalt-type analogs (e.g., layered, spinel-like, γ-$LiFeO_2$) with cation/anion ratio = 1, a wide range of ordered structures with distinct crystallographic features can exist. The feasibility of these structures depends on both the average oxidation state of the metal sites and the overall cation/anion ratio within the range of 1 to 2. In this space, different types of ordering between tetrahedrally and octahedrally coordinated metals emerge. Many of these structures retain an FCC oxygen sublattice. To accommodate an excess of cations relative to anions, some or all of the cations must occupy the tetrahedral interstitials of the oxygen sublattice. For example, to achieve a Li_2MO_2 stoichiometry, 2/3 of the total cations (e.g., all Li^+ in Li_2MO_2) occupy tetrahedral sites, resulting in a crystal structure with alternating layers of octahedrally and tetrahedrally coordinated cations. Li_2NiO_2 exemplifies such a structure [27]. When the cation/anion ratio is fixed at 3:2 and the oxidation state of M is +3, all species are likely forced into tetrahedral sites, as in Li_5FeO_4 [28]. Similarly, for a cation/anion ratio of 3:2 with M^{4+}, a structure such as Li_8SnO_6 arises [29], where 3/4 of the Li^+ ions occupy tetrahedral sites. This arrangement also exhibits alternating layers of octahedrally and tetrahedrally coordinated cations.

In addition to the scenarios described above, another way to achieve a cation/anion ratio >1 is through the formation of ordered oxygen vacancies within an otherwise perfect FCC oxygen sublattice. $Li_8Nb_2O_9$ [30] falls into this category, featuring no tetrahedrally coordinated cations but with approximately 10% oxygen vacancies relative to a full FCC oxygen sublattice. It is also worth noting that not all compounds with cation/anion ratios greater than one adopt an FCC-based oxygen sublattice or its analogs. For instance, Li_4GeO_4 [31] and Li_6TeO_6 [32] exhibit distinct crystalline frameworks that deviate from those discussed above. Given this rich diversity of crystallographic features, it is anticipated that isovalent ion substitution could enable the discovery of previously unreported ordered compounds within this compositional space. By following the described pipeline in Fig. 1(a), 13 and 245 calculations are generated.

3.2. New ground-state compounds and phase diagrams

To analyze the 13,245 computed compounds generated by the high-throughput pipeline, we first summarize the newly identified ground states absent from the Materials Project databases (as of July 2025) in Tables 2 and 3. Table 2 highlights the new ground states identified through GGA/GGA + U-level calculations, documenting their compositions, space groups, discovery pathways (e.g., via substitution of experimental entries, MP ground states, or prototype structures), cation/anion ratios, and whether these compounds have been reported experimentally. In total, 36 new ground states were discovered through this data-mining effort. Of these ground-state compounds, 15 exhibit cation/anion ratios >1, reinforcing the hypothesis that this compositional domain may exist in many yet undiscovered ground states. Furthermore, a literature survey revealed that Na_3TaO_4 (*C*2/*m*) [34] and Na_2HfO_3 (*C*2/*c*) [33], while absent from the Materials Project, have been experimentally reported. This observation further underscores the potential of

Table 2
New ground-state compounds identified through GGA/GGA + U.

No.	Compositions (Space Group)	Prototype Structure	Cation/anion ratios	Reported?
1	$Na_{14}Zn_2O_9$ (P $\bar{3}$)	$Na_{14}Mn_2O_9$ (mp-27569)	1.78	No
2	$Na_{14}Mg_2O_9$ (P $\bar{3}$)	$Na_{14}Mn_2O_9$ (mp-27569)	1.78	No
3	Na_5GaO_4 (*Pmmn*)	Na_5InO_4 (mp-8840)	1.50	No
4	Na_5FeO_4 (*Pmmn*)	Na_5InO_4 (mp-8840)	1.50	No
5	Li_2PbO_2 (*Pbcn*)	Na_2PbO_2 (mp-27622)	1.50	No
6	Na_5ScO_4 (*Pbca*)	Na_5InO_4 (mp-8840)	1.50	No
7	Li_3SbO_3 (P $\bar{1}$)	Li_3BiO_3 (mp-28510)	1.33	No
8	Na_3GaO_3 (*Cc*)	Na_3FeO_3 (mp-558570)	1.33	No
9	Na_5SbO_5 (*C*2/*c*)	Na_5TaO_5 (mp-8957)	1.20	No
10	Li_6MoO_6 (R $\bar{3}$)	Li_6TeO_6 (mp-7941)	1.17	No
11	Li_6WO_6 (R $\bar{3}$)	Li_6TeO_6 (mp-7941)	1.17	No
12	Na_6TeO_6 (R $\bar{3}$)	Na_6TeO_6 (prototype)	1.17	No
13	Na_6WO_6 (R $\bar{3}$)	Na_6TeO_6 (prototype)	1.17	No
14	$Na_5CuW_3O_8$ (P1)	$Na_5Co_4O_8$ (prototype)	1.12	No
15	$Li_8Ta_2O_9$ (P $\bar{1}$)	$Li_8Nb_2O_9$ (mp-28030)	1.11	No
16	Li_2FeO_3 (*C*2/*c*)	Na_2ZrO_3 (mp-990440)	1.00	No
17	Li_2CoO_3 (*C*2/*c*)	Na_2ZrO_3 (mp-990440)	1.00	No
18	$LiMnO_2$ (*P*2$_1$/*c*)	$LiYO_2$ (mp-7020)	1.00	No
19	Li_2MnO_3 (*C*2/*c*)	Na_2ZrO_3 (mp-990440)	1.00	No
20	Na_3TaO_4 (*C*2/*m*)	Na_3NbO_4 (mp-27247)	1.00	ICSD-789 [33]
21	Na_2TiO_3 (*Cmc*2$_1$)	Na_2GeO_3 (mp-5784)	1.00	No
22	Li_3TaO_4 (*P*2/*c*)	Na_3SbO_4 (mp-7404)	1.00	No
23	Na_2HfO_3 (*C*2/*c*)	Na_2ZrO_3 (mp-990440)	1.00	Cheung [33]
24	Na_2MnO_3 (*C*2/*c*)	Na_2ZrO_3 (mp-990440)	1.00	No
25	$LiCuO_2$ (*P*2$_1$/*c*)	$LiYO_2$ (mp-7020)	1.00	No
26	Li_3NbO_4 (*Pmn*2$_1$)	Li_3VO_4 (mp-19219)	1.00	No
27	Na_4MoO_5 (P $\bar{1}$)	Na_4TeO_5 (mp-15391)	1.00	No
28	$Na_3Ga_5O_9$ (*C*2/*c*)	$Na_3Fe_5O_9$ (mp-540658)	0.89	No
29	$Li_2Sb_4O_7$ (*C*2/*c*)	$Na_2Sb_4O_7$ (mp-30972)	0.86	No
30	Li_2WO_4 (*P*4$_1$22)	Li_2TeO_4 (mp-13843)	0.75	No
31	Na_2WO_4 (*P*2$_1$/*c*)	Na_2TeO_4 (mp-560613)	0.75	No
32	$Na_2Co_3O_7$ (P $\bar{1}$)	$Na_2Mn_3O_7$ (mp-19080)	0.71	No
33	Co_2O_3 (R $\bar{3}$ c)	Cr_2O_3 (mp-19399)	0.67	No
34	$LiTa_3O_8$ (*P*2$_1$/*c*)	$LiNb_3O_8$ (mp-3368)	0.50	No
35	$NaTa_{13}O_{33}$ (*C*2/*m*)	$NaNb_{13}O_{33}$ (mp-1203846)	0.42	No
36	Ta_2O_5 (P2)	Nb_2O_5 (mp-581967)	0.40	No

Table 3
New ground-state compounds identified through r^{2}SCAN.

No.	Compositions (Space Group)	Prototype Structure	Cation/anion ratios	Reported?
1	Na_5GaO_4 (*Pmmn*)	Na_5InO_4 (mp-8840)	1.50	No
2	Na_2MnO_2 (*Immm*)	Li_2FeO_2 (mp-755094)	1.50	No
3	Na_3NiO_3 (*Cmce*)	Na_3CuO_3 (mp-28556)	1.33	No
4	Li_3SbO_3 (P $\bar{1}$)	Li_3BiO_3 (mp-28510)	1.33	No
5	$Na_7Ga_3O_8$ (P $\bar{1}$)	$Na_7Al_3O_8$ (mp-556168)	1.25	No
6	Na_5SbO_5 (*C2/c*)	Na_5NbO_5 (mp-5477)	1.20	No
7	Na_6TeO_6 (R $\bar{3}$)	Na_6TeO_6 (prototype)	1.17	No
8	Li_6WO_6 (R $\bar{3}$)	Li_6TeO_6 (mp-7941)	1.17	No
9	$Li_8Ta_2O_9$ (P $\bar{1}$)	$Li_8Nb_2O_9$ (mp-28030)	1.11	No
10	$LiNiO_2$ (*C2/c*)	$NaYO_2$ (mp-30980)	1.00	No
11	$LiMnO_2$ (*P2$_1$/c*)	$LiYO_2$ (mp-7020)	1.00	No
12	Li_2GeO_3 (*C2/c*)	Li_2TiO_3 (mp-2931)	1.00	No
13	$NaVO_2$ (*P6$_3$/mmc*)	$LiNbO_2$ (mp-3924)	1.00	No
14	Li_3TaO_4 (I $\bar{4}$ 3m)	Li_3NbO_4 (mp-31488)	1.00	No
15	Na_2TiO_3 (*C2/c*)	Li_2CrO_3 (mp-755795)	1.00	No
16	$LiVO_2$ (*P6$_3$/mmc*)	$NaNbO_2$ (mp-3744)	1.00	No
17	Na_2HfO_3 (*C2/c*)	Na_2ZrO_3 (mp-990440)	1.00	Cheung [33]
18	Na_4MoO_5 (P $\bar{1}$))	Na_4WO_5 (mp-19334)	1.00	No
19	Li_2CoO_3 (*C2/c*)	Li_2SnO_3 (mp-3540)	1.00	No
20	$NaCuO_2$ (*P2$_1$/c*)	$LiYO_2$ (mp-7020)	1.00	No
21	FeO (P $\bar{6}$ m2)	MgO (mp-1009129)	1.00	No
22	NiO (*C2/c*)	AgO (mp-1065190)	1.00	No
23	Na_3TaO_4 (*C2/m*)	Na_3NbO_4 (mp-27247)	1.00	ICSD-789 [33]
24	$LiCuO_2$ (*P2$_1$/c*)	$LiYO_2$ (mp-7020)	1.00	No
25	Li_2SnO_3 (*C2/c*)	Li_2ZrO_3 (mp-4156)	1.00	No
26	$NaTiO_2$ (*Cm*)	$LiNiO_2$ (mp-2348641)	1.00	No
27	$Na_3Ga_5O_9$ (*C2/c*)	$Na_3Fe_5O_9$ (mp-540658)	0.89	No
28	$Li_2Sb_4O_7$ (*C2/c*)	$Na_2Sb_4O_7$ (mp-30972)	0.86	No
29	$NaFe_3O_5$ (*Pnma*)	$NaNi_3O_5$ (mp-1101477)	0.80	No
30	$NaGa_3O_5$ (*Pnnm*)	$NaFe_3O_5$ (mp-505170)	0.80	No
31	$Li_4Ni_5O_{12}$ (*C2/c*)	$Li_4Mn_5O_{12}$ (mp-691115)	0.75	No
32	$Li_4Co_5O_{12}$ (*C2/c*)	$Li_4Mn_5O_{12}$ (mp-691115)	0.75	No
33	Na_2TeO_4 (*P4$_1$22*)	Li_2TeO_4 (mp-13843)	0.75	No
34	$Na_2Ni_3O_7$ (P $\bar{1}$)	$Na_2Mn_3O_7$ (mp-19080)	0.71	No
35	$Na_2Co_3O_7$ (P $\bar{1}$)	$Na_2Mn_3O_7$ (mp-19080)	0.71	No
36	$Na_2Fe_3O_7$ (*P2$_1$/m*)	$Na_2Ti_3O_7$ (mp-3488)	0.71	No
37	$LiVO_3$ (R $\bar{3}$)	$LiNbO_3$ (mp-1078377)	0.67	No
38	Ni_2O_3 (R $\bar{3}$ c)	Cr_2O_3 (mp-19399)	0.67	No
39	Co_2O_3 (R $\bar{3}$ c)	In_2O_3 (mp-22323)	0.67	No
40	$Na_2V_6O_{13}$ (*C2/m*)	$Na_2Ti_6O_{13}$ (mp-5449)	0.62	No
41	$Li_2Mo_2O_7$ (P $\bar{1}$)	$Li_2W_2O_7$ (mp-27130)	0.57	No
42	$NaNb_3O_8$ (*P2$_1$/c*)	$LiNb_3O_8$ (mp-3368)	0.50	No
43	CoO_2 (*Pnnm*)	SnO_2 (mp-550172)	0.50	No
44	$LiTa_3O_8$ (*P2$_1$/c*)	$LiNb_3O_8$ (mp-3368)	0.50	No
45	$NaTa_3O_8$ (*C2/c*)	$LiTa_3O_8$ (mp-7638)	0.50	No

our data-mining approach to uncover experimentally synthesizable compounds.

Similarly, the newly identified ground states based on the r^{2}SCAN functional are summarized in Table 3. In contrast to the GGA/GGA + U ground states, 45 new ground states were discovered using the r^{2}SCAN functional. Notably, both Na_3TaO_4 (*C2/m*) and Na_2HfO_3 (*C2/c*), which are absent from the Materials Project database but reported in the literature, are also identified as r^{2}SCAN ground states. Furthermore, 34 new compounds are predicted to be ground states on the r^{2}SCAN convex hull but not on the GGA/GGA + U hull, highlighting the sensitivity of phase stability predictions to the exchange–correlation functional. As a meta-GGA functional, r^{2}SCAN generally provides more reliable phase-stability predictions for metal oxides, while being computationally more expensive than GGA(+U) [35–38]. Conversely, 23 compounds appear only as GGA/GGA + U ground states. Finally, 13 compounds are identified as ground states in both GGA/GGA + U and r^{2}SCAN calculations, further reinforcing their likelihood of being experimentally synthesizable. Using both functionals therefore allows us to assess functional sensitivity across chemical spaces and to provide guidance for future researchers on choosing the most appropriate functionals for the compounds we covered. Furthermore, all compounds reported on either convex hull exhibit sufficiently low E_{hull} values, suggesting they can be relatively easily stabilized according to remanent stability theory [10, 39–41]. Moreover, oxidation-state consistency for all compounds was verified by checking the magnetic moments of all cation sites, following the methodology established in our prior research [41–43], ensuring that identified compounds are chemically reasonable.

To demonstrate representative examples of the convex hull, we use the Na-Ta-O and Na-Ga-O systems as examples. Fig. 2(a)-(c) demonstrate the newly established GGA/GGA + U phase diagrams, r^{2}SCAN phase diagrams, and the Materials Project GGA/GGA + U phase diagrams for the Na-Ta-O space. Fig. 2(d)-(f) illustrate the same three phase diagrams for the Na-Ga-O space. Both the ground states and metastable states are illustrated in the phase diagram. The color bar on the left of each phase diagram indicates the color scheme of metastable states using the E_{hull} as a metric. Both Fig. 2(a)-(b) and Fig. 2(d)-(e) suggest that many more compounds are presented in these phase diagrams, in comparison to the Materials Project phase diagrams shown in Fig. 2(c) and (f). Specifically, Na_3TaO_4 shows up in both Fig. 2(a) and (b) but not Fig. 2(c). $NaTa_{13}O_{33}$ turns out to be the GGA/GGA + U ground state, whereas $NaTa_3O_8$ is found to be an r^{2}SCAN ground state. When it comes to the Na-Ga-O system, the Materials Project tends to have a relatively empty convex hull (see Fig. 2(f)). In contrast, it is identified in Fig. 2(d) that Na_3GaO_3 and $Na_3Ga_5O_9$ are the GGA/GGA + U ground states while $Na_7Ga_3O_8$, $Na_3Ga_5O_9$ and $NaGa_3O_5$ are the r^{2}SCAN ground states.

3.3. Metal dependency and trends across cation/anion ratio

In addition to the statistics of DFT computed ground states, the

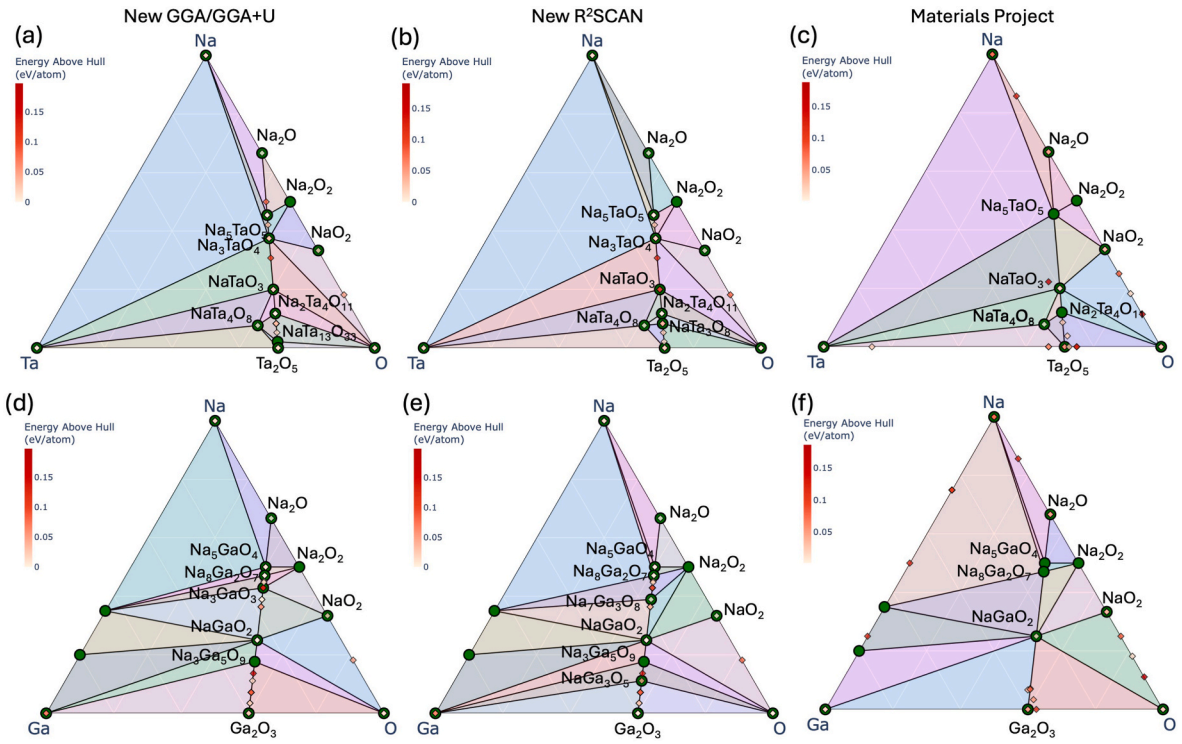

Fig. 2. Comparisons of the newly constructed convex hulls with the Materials Project convex hulls. (a–c) show the Na–Ta–O system using (a) GGA/GGA + U, (b) r^{2}SCAN, and (c) the Materials Project data. (d–f) show the Na–Ga–O system using (d) GGA/GGA + U, (e) r^{2}SCAN, and (f) the Materials Project data. Green circles represent stable compounds.

remanent stability conjecture [39] suggests that materials with relatively low E_{hull} could also be synthesizable. A reasonable upper bound of the E_{hull} value for metal oxides was suggested to be around 100 meV/atom by Sun et al. [39]. This empirical threshold is supported by a

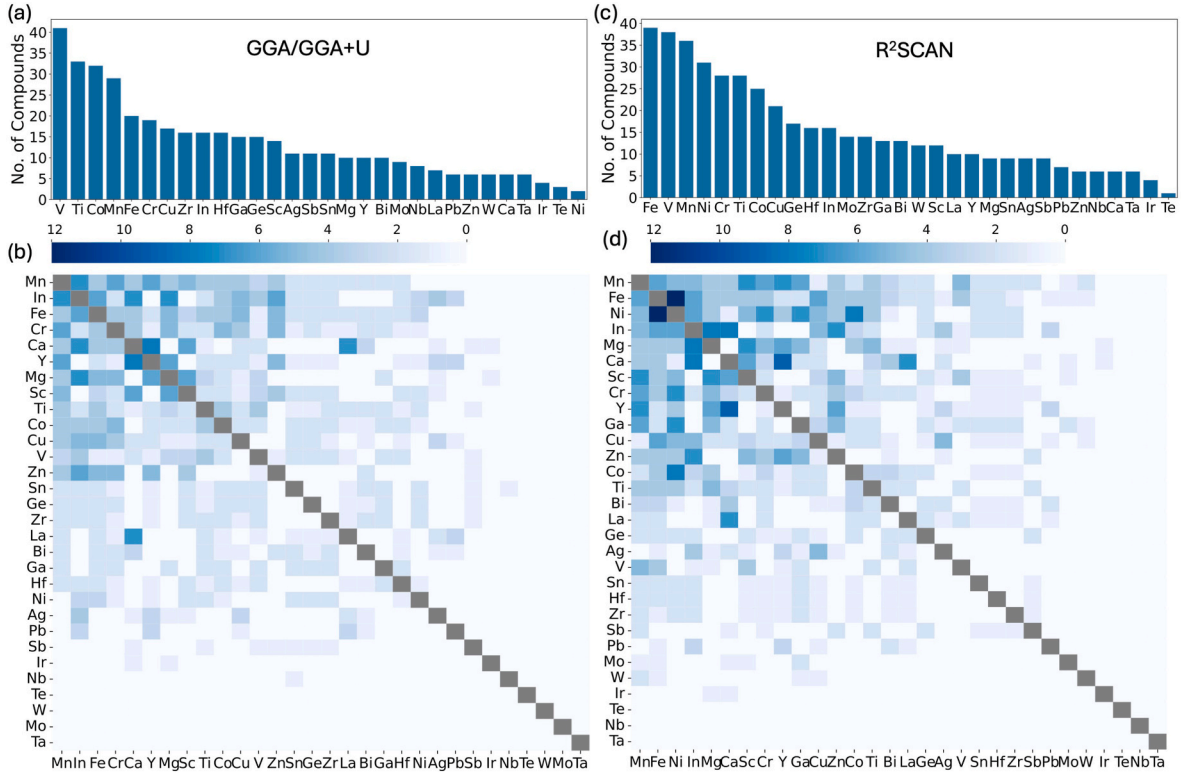

Fig. 3. Number of new compounds with E_{hull} < 100 meV/atom for: (a) GGA/GGA + U calculations on Li(Na)M_xO_y; (b) GGA/GGA + U calculations on Li(Na)$M_{x1}M'_{x2}O_y$; (c) r^{2}SCAN calculations on Li(Na)M_xO_y; (d) r^{2}SCAN calculations on Li(Na)$M_{x1}M'_{x2}O_y$. The heatmaps in (b) and (d) are sorted descending based on the total numbers in each column.

statistical analysis of ICSD-reported compounds, and subsequent experimental studies have further validated its broad applicability, making it a useful guideline for the experimental design of new Li/Na battery materials. Here we adopt this threshold to show the statistics of newly discovered metastable compounds with E_{hull} below 100 meV/atom in Fig. 3. Particularly, the metastable compounds with only one metal that is not Li or Na have been summarized in Fig. 3 (a) and (c) as bar plots, while metastable compounds with two metals are shown in Fig. 3(b) and (d) as heatmaps. In these heatmaps, the values at specific squares indicate the number of new metastable compounds discovered, with corresponding metals indicated by x and y axes. For all plots, we only show statistics for compounds that are not observed in the Materials Project database. As an overview, GGA/GGA + U calculations identified 409 newly discovered binary and ternary metal oxides, as well as 431 quaternary metal oxides. In contrast, r^{2}SCAN calculations identified 465 binary and ternary oxides and 514 quaternary oxides.

In addition to the overall statistics, several element-dependent trends can also be derived from Fig. 3. Many newly discovered ordered states have been observed in typical 3d metals used in Li-ion and Na-ion batteries, including Ti [44], V [45], Cr [46], Mn [47], Fe [45], Co [48], and Cu [45]. These species often exhibit complex energy landscape due to multiple (meta)stable oxidation states and rich magnetic behavior. Another major origin is that the versatility of oxidation number will also enable the variety of coordination environment that can be adapted to more structural framework. Moreover, it is worth noting that many metals, including some that are redox-active (such as Sn [49], Sb [50]) and those that are typically redox inactive (In [49], Ga [49], Te, and Hf) in battery application, have also shown a considerable number of metastable states.

Compounds containing such metals usually exhibit well-defined oxidation states and predictable paramagnetic or diamagnetic behavior, which reduces the likelihood of forming stable new phases. However, the observation of a few new compounds still reveals the potential to use these materials either as solid-state electrolytes or as charge compensators in electrode materials. The discovery of more ordered metastable states can be attributed to the fact that such metals are less studied, both computationally and experimentally.

In addition to metal dependency, it is also important to examine trends across different alkali metals and cation/anion ratios. These trends are analyzed and presented in Fig. 4, with GGA/GGA + U results shown in Fig. 4(a) and r^{2}SCAN results in Fig. 4(b). In both plots, the metastable compounds are grouped based on their cation/anion ratios. Ratios within (0, 0.5] primarily correspond to MO_x compounds with minimal or no Li/Na content, which typically serve as end members in the Li_2O–MO_x convex hull. The range (0.5, 0.75] encompasses "highly Li/Na-deficient" compounds that can emerge during the deep charge state of Li-ion and Na-ion batteries. The ratio 0.75 is highlighted because it represents the most common stoichiometry among spinel or spinel-like structures. Similarly, the range (0.75, 1.0) includes "slightly Li/Na-deficient" compounds, reflecting the early charge states of these batteries. A cation/anion ratio of 1.0 corresponds to most pristine states of Li-ion and Na-ion batteries. Finally, all compounds with cation/anion ratios greater than one are grouped into the range (1.0, 2.0). As shown in Fig. 4, most newly discovered metastable compounds fall within this last group, highlighting an overlooked opportunity for new materials discovery. This promising design space is further emphasized by the comparison with metastable entries from the Materials Project in Fig. 4(a). As indicated by the open and filled bars in Fig. 4(a), the number of newly discovered metastable compounds with cation/anion ratio $\leq$1 is significantly smaller than the number of existing entries. In contrast, a

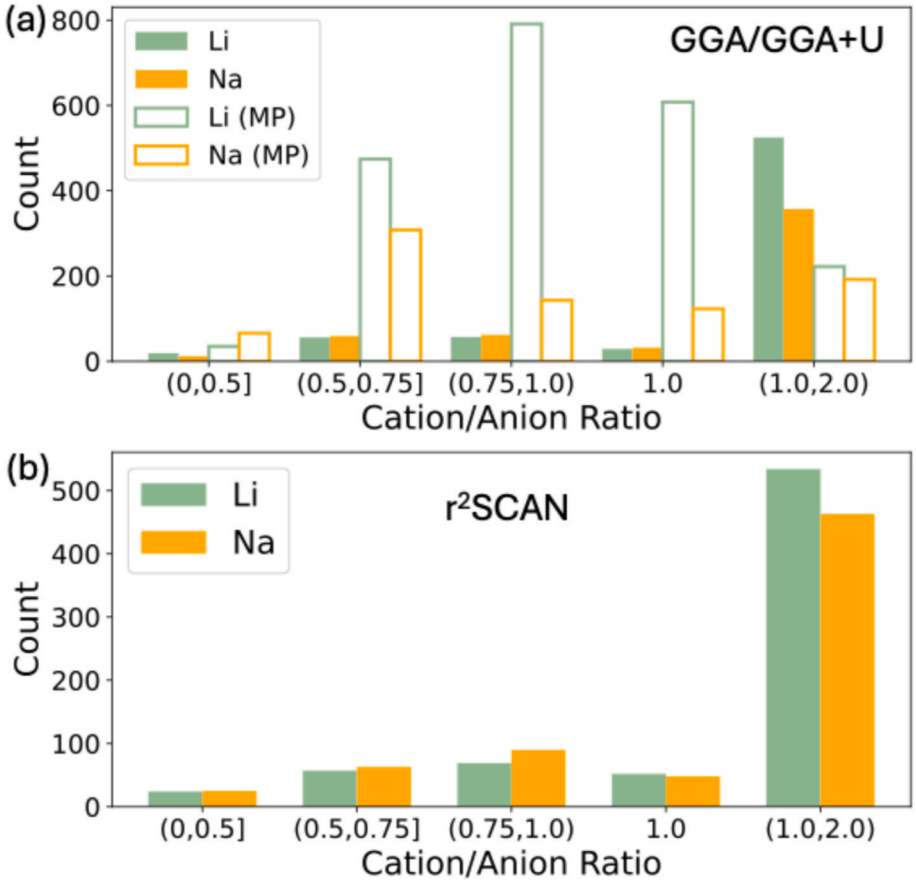

Fig. 4. Cation/anion ratio dependence and Li/Na dependence of new metastable compounds (E_{hull} < 100 meV/atom) for (a) GGA/GGA + U and (b) r^{2}SCAN. For (a), the open bars indicate the existing number of metastable entries in the Materials Project database.

substantial number of new compounds with cation/anion ratio >1 have been identified for both Li and Na metal oxides, especially when compared to the corresponding entries in the Materials Project. Particularly, there are 414 compounds with cation/anion ratios larger than one in the Materials Project, our data mining efforts identified another 882 compounds (525 Li metal oxides and 357 Na metal oxides) on top of it.

4. Conclusions

To summarize, we present a systematic data-mining effort aimed at discovering new ordered binary, ternary, and quaternary metal oxides that can be potentially used in Li-ion or Na-ion batteries. Ordered refers to a crystallographic arrangement in which different types of cations (e.g., Li or Na and transition metals) occupy distinct and predictable crystallographic sites within the crystal structure. High-throughput DFT calculations performed in this study have contributed to a dataset of 13,245 compounds, generated through isovalent substitution of ground states, experimentally reported entries, and specific prototype structures. Beyond identifying 36 new ground states within the GGA/GGA + U convex hull and 45 new ground states within the r^2SCAN convex hull, we also reveal an overlooked design space with cation/anion ratios greater than one, highlighting its potential for new materials discovery.

CRediT authorship contribution statement

Xiaozhao Liu: Data curation, Formal analysis, Investigation, Writing – original draft, Writing – review & editing. **Lin Wang:** Data curation, Formal analysis, Investigation, Writing – review & editing. **Benjamin Cahill:** Data curation, Formal analysis, Investigation, Writing – review & editing. **Hui Xiong:** Resources, Writing – original draft, Writing – review & editing. **Bin Ouyang:** Conceptualization, Data curation, Formal analysis, Investigation, Writing – original draft, Writing – review & editing. **Yan Zeng:** Conceptualization, Resources, Supervision, Writing – original draft, Writing – review & editing.

Declaration of competing interest

The authors declare that they have no known competing financial interests or personal relationships that could have appeared to influence the work reported in this paper.

Acknowledgements

The work on Na metal oxides was supported by the Office of Vehicle Technologies of the U.S. Department of Energy through the Advanced Battery Materials Research (BMR) Program (LENS Consortium). The work on Li metal oxides was supported by the startup fund and First Year Assistant Professor Grant from Florida State University awarded to Y.Z. and the CRC Seed Grant from Florida State University awarded to B.O. The work from H.X. was supported by the U.S. Department of Energy, Office of Science, Office of Basic Energy Sciences program under Award Number DE-SC0019121. Computational resources were provided by the Advanced Cyberinfrastructure Coordination Ecosystem: Services & Support (ACCESS), the National Energy Research Scientific Computing Center (NERSC), a DOE Office of Science User Facility supported by the Office of Science and the U.S. Department of Energy under contract no. DE-AC02-05CH11231, and the Research Computing Center (RCC) at Florida State University. The computation and data processing were also supported by the supercomputing resources from the Department of Energy's Office of Energy Efficiency and Renewable Energy at the National Renewable Energy Laboratory. We thank Dr. Yufang He for her input to the manuscript. We also thank Dr. Christopher Stiles Johnson for the fruitful discussions.

Appendix A. Supplementary data

Supplementary data to this article can be found online at https://doi.org/10.1016/j.mtener.2026.102253.

Data availability

Data will be made available on request.

References

[1] Materials genome initiative. https://www.mgi.gov/. (Accessed 9 October 2025).
[2] A. Urban, D.-H. Seo, G. Ceder, Computational understanding of Li-ion batteries, npj Comput. Mater. (2) (2016) 16002, https://doi.org/10.1038/npjcompumats.2016.2.
[3] A. Jain, S.P. Ong, G. Hautier, W. Chen, W.D. Richards, S. Dacek, S. Cholia, D. Gunter, D. Skinner, G. Ceder, K.A. Persson, Commentary: the materials project: a materials genome approach to accelerating materials innovation, APL Mater. (1) (2013) 011002, https://doi.org/10.1063/1.4812323.
[4] J.E. Saal, S. Kirklin, M. Aykol, B. Meredig, C. Wolverton, Materials design and discovery with high-throughput density functional theory: the open quantum materials database (OQMD), JOM (65) (2013) 1501–1509, https://doi.org/10.1007/s11837-013-0755-4.
[5] S. Curtarolo, W. Setyawan, G.L.W. Hart, M. Jahnatek, R.V. Chepulskii, R.H. Taylor, S.D. Wanga, J.K. Xue, K.S. Yang, O. Levy, M.J. Mehl, H.T. Stokes, D.O. Demchenko, D. Morgan, AFLOW: an automatic framework for high-throughput materials discovery, Comput. Mater. Sci. 58 (2012) 218–226, https://doi.org/10.1016/j.commatsci.2012.02.005.
[6] C. Draxl, M. Scheffler, The NOMAD laboratory: from data sharing to artificial intelligence, Journal of Physics-Materials (2) (2019) 36001, https://doi.org/10.1088/2515-7639/ab13bb.
[7] Y. Tian, G. Zeng, A. Rutt, T. Shi, H. Kim, J. Wang, J. Koettgen, Y. Sun, B. Ouyang, T. Chen, Z. Lun, Z. Rong, K. Persson, G. Ceder, Promises and challenges of next-generation "beyond Li-ion" batteries for electric vehicles and grid decarbonization, Chem. Rev. 121 (2021) 1623–1669, https://doi.org/10.1021/acs.chemrev.0c00767.
[8] A. Jain, Y. Shin, K.A. Persson, Computational predictions of energy materials using density functional theory, Nat. Rev. Mater. (1) (2016) 15004, https://doi.org/10.1038/natrevmats.2015.4.
[9] Z. Lun, B. Ouyang, D.H. Kwon, Y. Ha, E.E. Foley, T.Y. Huang, Z. Cai, H. Kim, M. Balasubramanian, Y. Sun, J. Huang, Y. Tian, H. Kim, B.D. McCloskey, W. Yang, R.J. Clement, H. Ji, G. Ceder, Cation-disordered rocksalt-type high-entropy cathodes for Li-ion batteries, Nat. Mater. 20 (2021) 214–221, https://doi.org/10.1038/s41563-020-00816-0.
[10] L. Wang, J. Wang, B. Ouyang, Computational investigation of MAX as intercalation host for rechargeable aluminum-ion battery, Adv. Energy Mater. (13) (2023) 2302584, https://doi.org/10.1002/aenm.202302584.
[11] Y. He, Z. He, B. Ouyang, Design principle of disordered rocksalt type overlithiated anode for high energy density batteries, Mater. Horiz. (2024), https://doi.org/10.1039/D4MH00715H.
[12] L. Wang, T. He, B. Ouyang, Impact of domain knowledge on the property prediction of specialized machine learning models, ACS Mater. Lett. (2025) 2708–2715, https://doi.org/10.1021/acsmaterialslett.5c00726.
[13] Z. Cai, B. Ouyang, H.-M. Hau, T. Chen, R. Giovine, K.P. Koirala, L. Li, H. Ji, Y. Ha, Y. Sun, J. Huang, Y. Chen, V. Wu, W. Yang, C. Wang, R.J. Clément, Z. Lun, G. Ceder, *In situ* formed partially disordered phases as earth-abundant Mn-rich cathode materials, Nat. Energy (2023), https://doi.org/10.1038/s41560-023-01375-9.
[14] L. Wang, Z. He, B. Ouyang, Data driven design of compositionally complex energy materials, Comput. Mater. Sci. 230 (2023) 112513, https://doi.org/10.1016/j.commatsci.2023.112513.
[15] T.-L. Pham, L. Wang, B. Ouyang, Design principle for anode stable solid-state electrolytes, J. Mater. Chem. A (2024), https://doi.org/10.1039/D4TA02269F.
[16] M.J. Dheerasinghe, Y. Gan, L. Wang, Y. He, Z. He, G. Xu, Y. Zhao, B. Ouyang, High throughput screening of high entropy spinel electrolytes for multivalent batteries, Chem. Commun. (2025), https://doi.org/10.1039/D5CC02095F.
[17] Y. Zeng, B. Ouyang, J. Liu, Y.-W. Byeon, Z. Cai, L.J. Miara, Y. Wang, G. Ceder, High-entropy mechanism to boost ionic conductivity, Science 378 (2022) 1320–1324, https://doi.org/10.1126/science.abq1346.
[18] Y. He, E. Scivally, A. Shaji, B. Ouyang, Y. Zeng, Unraveling the fast ionic conduction in NASICON-Type materials, Adv. Energy Mater. 15 (2025) 2403877, https://doi.org/10.1002/aenm.202403877.
[19] S.P. Ong, L. Wang, B. Kang, G. Ceder, Li-Fe-P-O phase diagram from first principles calculations, Chem. Mater. 20 (2008) 1798–1807, https://doi.org/10.1021/cm702327g.
[20] J. Hafner, G. Kresse, The vienna AB-Initio Simulation Program VASP: an efficient and versatile tool for studying the structural, dynamic, and electronic properties of materials, in: A. Gonis, A. Meike, P.E.A. Turchi (Eds.), Properties of Complex Inorganic Solids, Springer US, Boston, MA, 1997, pp. 69–82.
[21] G. Kresse, J. Furthmüller, Efficient iterative schemes for *ab initio* total-energy calculations using a plane-wave basis set, Phys. Rev. B (54) (1996) 11169–11186, https://doi.org/10.1103/PhysRevB.54.11169.

[22] J.P. Perdew, K. Burke, M. Ernzerhof, Generalized gradient approximation made simple, Phys. Rev. Lett. (77) (1996) 3865–3868, https://doi.org/10.1103/PhysRevLett.77.3865.
[23] J.W. Furness, A.D. Kaplan, J. Ning, J.P. Perdew, J. Sun, Accurate and numerically efficient r^{2}SCAN meta-generalized gradient approximation, J. Phys. Chem. Lett. (11) (2020) 8208–8215, https://doi.org/10.1021/acs.jpclett.0c02405.
[24] J. Sun, R.C. Remsing, Y. Zhang, Z. Sun, A. Ruzsinszky, H. Peng, Z. Yang, A. Paul, U. Waghmare, X. Wu, M.L. Klein, J.P. Perdew, Accurate first-principles structures and energies of diversely bonded systems from an efficient density functional, Nat. Chem. (8) (2016) 831–836, https://doi.org/10.1038/nchem.2535.
[25] S.L. Dudarev, G.A. Botton, S.Y. Savrasov, C.J. Humphreys, A.P. Sutton, Electron-energy-loss spectra and the structural stability of nickel oxide: an LSDA+U study, Phys. Rev. B (57) (1998) 1505–1509, https://doi.org/10.1103/PhysRevB.57.1505.
[26] L. Wang, T. Maxisch, G. Ceder, Oxidation energies of transition metal oxides within the GGA+U framework, Phys. Rev. B (73) (2006) 195107, https://doi.org/10.1103/PhysRevB.73.195107.
[27] K. Kang, C.-H. Chen, B.J. Hwang, G. Ceder, Synthesis, electrochemical properties, and phase stability of Li_2NiO_2 with the *Immm* structure, Chem. Mater. (16) (2004) 2685–2690, https://doi.org/10.1021/cm049922h.
[28] C.S. Johnson, S.H. Kang, J.T. Vaughey, S.V. Pol, M. Balasubramanian, M. M. Thackeray, Li_2O removal from Li_5FeO_4: a cathode precursor for lithium-ion batteries, Chem. Mater. 22 (2010) 1263–1270, https://doi.org/10.1021/cm902713m.
[29] N. Kuganathan, A.L. Solovjov, R.V. Vovk, A. Chroneos, Defects, diffusion and dopants in Li_8SnO_6, Heliyon (7) (2021) e07460, https://doi.org/10.1016/j.heliyon.2021.e07460.
[30] R.M. Braun, R. Hoppe, Zur Kenntnis von $Li_{16}Nb_4O_{18}$ [1], Z. Anorg. Allg. Chem. 493 (2004) 7–16, https://doi.org/10.1002/zaac.19824930102.
[31] H. Völlenkle, A. Wittmann, Zur Kristallstruktur von Li_4SiO_4 und Li_4GeO_4, Naturwissenschaften (54) (1967) 441, https://doi.org/10.1007/bf00603145, 441.
[32] T. Wisser, R. Hoppe, On oxotellurates(VI) of the alkali metals. Existence and constitution of Li_6TeO_6. Neues ueber oxotellurate(VI) der alkalimetalle. Zur existenz und konstitution von Li_6TeO_6, Z. Fuer Anorg. Allg. Chem. (1989) 573, ger. Democr. Repub.).
[33] R. Chang, E. Svensson Grape, T. Clairefond, E. Tikhomirov, A.K. Inge, O. Cheung, Synthesis and characterization of sodium hafnium oxide (Na_2HfO_3) and its high-temperature CO_2 sorption properties, J. Mater. Chem. A (11) (2023) 7617–7628, https://doi.org/10.1039/d3ta00415e.
[34] M.-C. Illy, A.L. Smith, G. Wallez, P.E. Raison, R. Caciuffo, R.J.M. Konings, Thermal expansion of the nuclear fuel-sodium reaction product $Na_3(U_{0.84(2)},Na_{0.16(2)})O_4$ - structural mechanism and comparison with related sodium-metal ternary oxides, J. Nucl. Mater. 490 (2017) 101–107, https://doi.org/10.1016/j.jnucmat.2017.03.045.
[35] M. Kothakonda, A.D. Kaplan, E.B. Isaacs, C.J. Bartel, J.W. Furness, J. Ning, C. Wolverton, J.P. Perdew, J. Sun, Testing the r^{2}SCAN density functional for the thermodynamic stability of solids with and without a van der waals correction, ACS Mater. Au (3) (2023) 102–111, https://doi.org/10.1021/acsmaterialsau.2c00059.
[36] R. Kingsbury, A.S. Gupta, C.J. Bartel, J.M. Munro, S. Dwaraknath, M. Horton, K. A. Persson, Performance comparison of r^{2}SCAN and SCAN metaGGA density functionals for solid materials via an automated, high-throughput computational workflow, Phys. Rev. Mater. (6) (2022) 13801, https://doi.org/10.1103/PhysRevMaterials.6.013801.
[37] M.C. Kuner, A.D. Kaplan, K.A. Persson, M. Asta, D.C. Chrzan, MP-ALOE: an r^{2}SCAN dataset for universal machine learning interatomic potentials, npj Comput. Mater. 11 (2025) 352, https://doi.org/10.1038/s41524-025-01834-9.
[38] H. Liu, X. Bai, J. Ning, Y. Hou, Z. Song, A. Ramasamy, R. Zhang, Y. Li, J. Sun, B. Xiao, Assessing r^{2}SCAN meta-GGA functional for structural parameters, cohesive energy, mechanical modulus, and thermophysical properties of 3d, 4d, and 5d transition metals, J. Chem. Phys. 160 (2024) 24102, https://doi.org/10.1063/5.0176415.
[39] W. Sun, S.T. Dacek, S.P. Ong, G. Hautier, A. Jain, W.D. Richards, A.C. Gamst, K. A. Persson, G. Ceder, The thermodynamic scale of inorganic crystalline metastability, Sci. Adv. (2) (2016) e1600225, https://doi.org/10.1126/sciadv.1600225.
[40] B. Ouyang, J. Wang, T. He, C.J. Bartel, H. Huo, Y. Wang, V. Lacivita, H. Kim, G. Ceder, Synthetic accessibility and stability rules of NASICONs, Nat. Commun. (12) (2021) 5752, https://doi.org/10.1038/s41467-021-26006-3.
[41] L. Wang, N. Sunariwal, Y. He, D.-h. Kim, D.-h. Yeon, Y. Zeng, J. Cabana, B. Ouyang, Elemental stability rules for High Entropy disordered Rocksalt type Li-Ion battery positive electrodes, Adv. Energy Mater. (15) (2025) 2404982, https://doi.org/10.1002/aenm.202404982.
[42] Z.Y. Lun, B. Ouyang, Z.J. Cai, R. Clément, D.H. Kwon, J.P. Huang, J.K. Papp, M. Balasubramanian, Y.S. Tian, B.D. McCloskey, H.W. Ji, H. Kim, D.A. Kitchaev, G. Ceder, Design principles for high-capacity Mn-Based cation-disordered rocksalt cathodes, Chem (6) (2020) 153–168, https://doi.org/10.1016/j.chempr.2019.10.001.
[43] L. Wang, Y. Wang, J. Martin, E. Scivally, Z. He, D.-h. Kim, D.-h. Yeon, Y. Zeng, D. Chen, B. Ouyang, Origin of enhanced disorder in high entropy rocksalt type Li-ion battery cathodes, EES Batteries (1) (2025) 1731–1739, https://doi.org/10.1039/D5EB00104H.
[44] J. Bhattacharya, A. Van Der Ven, Phase stability and nondilute Li diffusion in spinel Li_{1+x} Ti_2O_4, Phys. Rev. B (81) (2010) 104304, https://doi.org/10.1103/PhysRevB.81.104304.
[45] S. Buta, D. Morgan, A.V.d. Ven, M.K. Aydinol, G. Ceder, Phase separation tendencies of aluminum-doped transition-metal oxides ($LiAl_{1-x}M_xO_2$) in the α - $NaFeO_2$ crystal structure, J. Electrochem. Soc. 146 (1999) 4335, https://doi.org/10.1149/1.1392639.
[46] J.L. Kaufman, A. Van der Ven, First-principles investigation of phase stability in layered Na_xCrO_2, Phys. Rev. Mater. (6) (2022) 115401, https://doi.org/10.1103/PhysRevMaterials.6.115401.
[47] G.E. García Ponte, S.S. Behara, E.N. Bassey, R.J. Clément, A. Van der Ven, First-principles statistical mechanics study of magnetic fluctuations and order–disorder in the spinel $LiNi_{0.5}Mn_{1.5}O_4$ cathode, Chem. Mater. (2025), https://doi.org/10.1021/acs.chemmater.4c02772.
[48] G. Ceder, A.F. Kohan, M.K. Aydinol, P.D. Tepesch, A. van der Ven, Thermodynamics of oxides with substitutional disorder: a microscopic model and evaluation of important energy contributions, J. Am. Ceram. Soc. (81) (1998) 517–525, https://doi.org/10.1111/j.1151-2916.1998.tb02369.x.
[49] S. Behara, J. Thomas, A. Van der Ven, A. Van der Ven, Fundamental thermodynamic, kinetic, and mechanical properties of lithium and its alloys, Chem. Mater. (36) (2024) 7370–7387, https://doi.org/10.1021/acs.chemmater.4c01279.
[50] D. Chang, M.-H. Chen, A. Van der Ven, Factors contributing to path hysteresis of displacement and conversion reactions in Li ion batteries, Chem. Mater. 27 (2015) 7593–7600, https://doi.org/10.1021/acs.chemmater.5b02356.